Available online at www.sciencedirect.com
SCIENCE DIRECT®
PERGAMON
International Journal of Multiphase Flow 29 (2003) 1265–1282
International Journal of Multiphase Flow
www.elsevier.com/locate/ijmulflow

The effects of viscosity on coalescence-induced coalescence

D. Stefan Martula, Roger T. Bonnecaze, Douglas R. Lloyd *

Department of Chemical Engineering, The University of Texas at Austin, Austin, TX 78712-1062, USA

Received 1 July 2002; received in revised form 15 May 2003

Abstract

The effects of variable matrix-phase viscosity on the rate of coarsening of relatively inviscid diluent droplets in a viscous polymer matrix are examined. Emulsions of low viscosity diphenyl ether (DPE) droplets in a viscous matrix mixture of isotactic polypropylene (iPP) and DPE are formed by thermal quenching of a homogeneous phase below the binodal. The droplets coarsen via the mechanism of coalescence-induced coalescence (CIC), where two coalescing droplets create a flow that drives other droplets to coalesce, thus creating a cascade process. Previous work on CIC indicate that the growth exponent of the average droplet size depends on the volume fraction of the diluent phase, but does not depend on the viscosity of the matrix phase or the DPE–iPP interfacial tension. Different iPP molecular weights in the experiments cause a variation in the viscosity, but practically no change in the interfacial tension nor in the phase behavior of the system. The growth exponent is found to not vary with the viscosity of the matrix phase, supporting the CIC theory.

Keywords: Coarsening; Droplets; Coalescence; Polymer solutions; Rheology

1. Introduction

Phase separation is a ubiquitous process that occurs in a variety of natural and engineered systems. Examples include thermally induced phase separation (TIPS) for the formation of microporous membranes, the formation of immiscible polymer blends, and liquid–liquid extraction. In TIPS for example, a homogeneous material is thermally quenched to form a two-phase mixture. The initial phase separation occurs either by nucleation and growth or spinodal decomposition (e.g., Siggia, 1979). The dynamics of subsequent droplet growth has a profound impact on

* Corresponding author. Tel.: +1-512-471-4985; fax: +1-512-471-7060.
E-mail address: lloyd@che.utexas.edu (D.R. Lloyd).

0301-9322/03/$ - see front matter
doi:10.1016/S0301-9322(03)00102-2

the morphology of the two-phase system, as it ultimately affects final domain dimensions, mechanical strength, and transport properties of materials formed via phase separation processes. In the later stages of binary phase separation, the components have distributed themselves either in a microstructure composed of two co-continuous phases or droplets of one phase in a continuous matrix of the other phase. Usually, the former morphology breaks up into droplets due to a capillary instability, and in either case the droplets coarsen in order to minimize the interfacial area and the total free energy of the system. The study reported here was concerned with this late-stage coarsening process.

Droplet coarsening can occur due to a variety of mechanisms, including gravitational creaming or settling (Zhang and Davis, 1991; Wang and Davis, 1995), convection due to chemical potential or concentration gradients (Santonicola et al., 2001), shear-induced collisions (Feke and Schowalter, 1983; Wang and Davis, 1995), evaporation–condensation (Lifshitz and Slyozov, 1961) or collisions due to Brownian diffusion (e.g., (Binder and Stauffer, 1976)). In the latter two mechanisms, the average droplet size $\langle a \rangle$ is predicted to grow according to $\langle a \rangle \sim t^{1/3}$ where t is time.

Recently, several investigators (Tanaka, 1994; McGuire et al., 1995; Nikolayev et al., 1996; Beysens, 1997) proposed a new mechanism, sometimes called coalescence-induced coalescence (CIC) or collision-induced collision. According to CIC, coarsening occurs as follows. In the late stages of phase separation, some pairs of droplets in the emulsion are sufficiently close that their interfaces interact strongly due to van der Waals forces. Ultimately, this attractive force causes instability in the thin film separating the droplets, resulting in the pair of droplets coalescing. This can be considered as coalescence beginning when the droplets are within some critical distance of one another. Initially, a small neck is formed between the pairs of droplets, and the starting "dumbell" shape of the coalescing pair relaxes due to capillary forces into a larger spherical droplet. In Tanaka's so-called "direct" CIC, the motion of the interface of a coalescing pair contacts another droplet beginning another coalescence. In Tanaka's so-called "indirect" CIC, the hydrodynamic flow created by the coalescing pair drives other pairs to coalesce, thus creating a cascade process. In these systems the droplet sizes range from 1 to 100 μm in fluids with viscosities ranging from a few centipoise to tens of poise. The interfacial tension can be as low as a fraction of a dyne/cm to tens of dynes/cm. Low-Reynolds-number hydrodynamics dominate these systems, with Reynolds number on the order of 10^{-8}–10^{-2}. The typical time scale for CIC in these studies ranges from tens of seconds to tens of minutes.

The growth exponent ξ for the growth rate of the average droplet size ($\langle a \rangle = At^{\xi}$), varies widely for supposed CIC systems. In some cases $\xi = 1$ for a volume fraction of the discontinuous droplet phase ϕ above a critical value ϕ_c ($\phi_c = 0.35$) (Perrot et al., 1994; Tanaka, 1994; Tanaka et al., 1994; Guenon et al., 1987; White and Wiltzius, 1995). For volume fractions less than the critical value $\xi = 1/3$ corresponding to what has been argued to be Brownian coagulation. These experiments are typically for liquid pairs of low, but similar viscosities (binary systems of cyclohexane–methanol or styrene–caprolactone oligomers) where buoyancy effects are very small and evaporation–condensation is not active. Some simple theories and models have been put forward to explain some aspects of this behavior (Beysens, 1997; Nikolayev and Beysens, 1997; Nikolayev et al., 1996). These researchers argue that the "direct" CIC mechanism is the most important and predict an exponent of unity. The precise dependence of the power-law prefactor A on the viscosity ratios, interfacial tension, and volume has not been determined due to the complexities of the multiphase flow with moving interfaces and long-range interparticle interactions.

Nikolayev et al. (1996) and Beysens (1997) model direct CIC by considering three droplets with cylindrical symmetry within a much larger spherical drop; the latter meant to model the effects of the surrounding emulsion. The three-dimensional nature of the flow and interdroplet interactions are not taken into account. Troian has argued that the walls in the viewing cells may be the cause of the growth exponent being close to unity in some of the experiments (Troian, 1993).

However, other power-law relationships have been observed for CIC as well. For quenches of polymer–diluent pairs (Brown and Chakrabarti, 1993; Song and Torkelson, 1995; McGuire et al., 1995) the values of ξ vary from 0.05 to 0.9, increasing with increasing volume fraction of the droplet phase. For these experiments, the buoyancy effects are very small due to the small density differences between the polymer and diluent and the high viscosity of the polymer-matrix phase. Further, in the case of McGuire et al. (1995) it has been shown (Martula et al., 2000) that the evaporation–condensation mechanism and Brownian coagulation are too slow compared to the observed time-scale (several minutes) for coarsening. For the polymer–diluent system, the droplets are low viscosity (almost inviscid) relative to the very viscous polymer matrix. It appears that the relative viscosities between the droplets and the matrix may influence the exponent, but the details are not clear.

Viscoelastic spinodal decomposition (Onuki, 2002) may also account for variations in the growth exponents. While the viscosity contrast between the diluent droplets and polymer-rich matrix, rheological measurements indicate that the fluids are still Newtonian. In addition we examine droplet growth long after phase separation is complete and the morphologies we observe are not like those seen in viscoelastic spinodal decomposition (Tanaka, 1996). Here we shall model the system as a viscous emulsion composed of two Newtonian fluids, where the volume fraction of the droplets remains constant throughout the coarsening process.

McGuire et al. (1996) put forth a semi-analytical model for "indirect" CIC based on an approximate model for the flow generated by a coalescence event and how that impacts the collision frequency among other pairs in an emulsion. The model includes an adjustable parameter for each volume fraction that allowed good agreement with experimental observations, but values of the parameter were not justifiable on physical grounds.

A Stokesian dynamics-like simulation of indirect CIC recently been developed in our group uses a realistic though approximate model of the coalescence-induced flow and interdroplet interactions (Martula et al., 2000). After placing droplets randomly in a periodically replicated three-dimensional box, the flow due to pairs of drops sufficiently close to coalesce was described by a ring of point forces. The ring strength and radius was estimated based on scaling laws, and the flow continued until the radius of the ring was equal to the radius of the new droplet and the coalescence was complete. The flow at any point was assumed to be the sum of the coalescence events, and the droplets were advanced according to Faxen's law. Any pairs of drops within the critical distance of coalescence would then be assumed to be coalescing, and thus generate a flow.

Using one adjustable parameter, which was set to a physically justifiable value, the simulation successfully predicted the average droplet size as a function of time and the variation in the exponents as a function of volume fraction. The predicted results compared favorably to the experiments on polymer–diluent systems with. Also, it was observed that ξ equaled approximately 0.5 and was independent of droplet phases volume fraction for volume fractions greater than about 0.5. The evolution of the size distribution of droplets was also determined. Comparisons with experimental data were very good.

The objective of this paper is to further test experimentally the CIC phenomena by varying the physical properties of the system. Specifically, the viscosity of the matrix phase is changed by varying the molecular weight of the polymer. While increasing the molecular weight of the polymer increases the viscosity of the continuous phase, it has little influence on the interfacial tension between the droplets and the matrix. The CIC mechanism predicts that for this system, the average size of the droplets as a function of time should be a function of only a normalized time (scaled proportionally with matrix viscosity) and the volume fraction of the droplet phase. The objective of the study reported here was to confirm this behavior, providing additional support for the CIC mechanism.

The outline of the paper is as follows. First, the materials for the CIC experiments are described. Then the measurement of the viscosity of the matrix phase and estimates of the interfacial tensions as a function of the polymer–diluent composition are reported. Next, the experiments and their results for measurement of the average droplet size as a function of time are reported. These data are then compared to the theoretical predictions of the scaling analysis and numerical simulation of Martula et al. (2000). Finally, the paper ends with some concluding remarks and observations.

2. Experimental materials and methods

The polymer–diluent system selected for this study was the same as that used previously (McGuire et al., 1995): isotactic polypropylene–diphenyl ether (iPP–DPE). Experiments in this study were conducted with two iPP samples: $M_w = 120{,}000$ g/mole (designated iPP120) and 138,000 g/mole (designated iPP138). The results were compared to those of McGuire et al., who used iPP of $M_w = 168{,}000$ g/mole (designated iPP168). DPE was selected in both studies because it has a high-boiling (532 K), which minimizes evaporation during the experiments. The iPP–DPE system is ideal for coarsening studies due to its large miscibility gap (Nakajima and Fujiwara, 1968) (allowing for experiments to be carried out at several different quench conditions), the difference in the refractive indices of the polymer-rich and polymer-lean phases (Laxminarayan, 1994) (allowing for easier viewing via optical microscopy), and its isopycnic character (ensuring that gravity does not accelerate the growth).

The viscosity η of a polymer solution has been shown to increase approximately as $M_w^{2/3}$ (Allcock and Lampe, 1990), but other parameters such as the interfacial tension γ (Anastasiadis et al., 1988) and the position of the iPP–DPE binodal curve (Batarseh, 1999; Atkinson, 1999) do not depend strongly on M_w. Thus, changing the M_w of iPP should have a significant effect on only one of the parameters believed to affect the coarsening of emulsions via CIC.

The polymers (both obtained from Exxon Chemical) and DPE (Aldrich, 99% purity) were used as received from the manufacturers without further purification. The polydispersity indices of the polymers are not known.

2.1. Coarsening experiments

iPP–DPE samples were prepared in a manner similar to that reported previously (Laxminarayan, 1994; McGuire, 1995; Atkinson, 1999). Appropriate amounts of polymer and diluent

were weighed into a 13 mm × 100 mm borosilicate test tube to a total mass of slightly less than 2 g. The tube was purged with nitrogen for 60 s, sealed using a propane–oxygen flame, and placed in a convection oven at 473 K for at least 48 h. The tube was dropped into liquid nitrogen for 30 s, retrieved, and broken open to yield a white solid cylindrical polymer–diluent sample. A coarsening experiment was initiated by placing a small piece (about 0.02 g) of sample between two glass cover slips. The cover slips were separated by a 50 μm thick Teflon spacer with a window cut in the center. Vacuum grease was used to seal the cover slip assembly, which provided a consistent sample volume upon melting and limited diluent evaporation during the experiment.

The assembly was placed on a hot stage (Linkam HFS-91) that rested on the platform of an optical microscope (Nikon Optiphot2-Pol). The hot stage, which had a rated maximum cooling rate of 130 K/min but a true maximum of approximately 100 K/min, was controlled with a Linkam TMS-91 controller and a Linkam CS-196 cooling unit. The thermal response time of the sample is on the order of 0.7 s (McGuire, 1995), which is much faster than the coarsening process. Thus, the temperature may be assumed to be uniform across the sample. The image from the microscope was converted into a video signal with a digital camera and controller (MTI CCD-72X). The signal was passed through a FOR.A video timer and into a S-VHS videocassette recorder (Panasonic AG-1960) where it was captured on an S-VHS videotape (FUJI ST-120) for subsequent image analysis. The optical microscope was fitted with a long focal length M Plan 60× objective lens. The length of the objective (and thus the magnification of the image) was limited by the presence of the hot stage. Experiments could be observed in real time on a video monitor; the image on the screen had a viewing area of 150 μm by 200 μm.

Initially, the sample was held at 433 K for 10 min to allow the sample to homogenize; preliminary experiments have been shown that this is sufficient to remove thermal history (Lim, 1990). Next, the hot stage was used to quench the sample into the liquid–liquid region at 100 K/min, inducing phase separation and coarsening. Recordings of the experiments were analyzed using an 8-bit black and white framegrabber (ITI-OFG) mounted in a 486-33 personal computer. BIOSCAN Optimas 3.0 digital image analysis software was used to determine the sizes of droplets, which could be discerned when they grew to a radius of 2 μm. At each selected measurement time, an image was frozen and the circumferences of at least 20 droplets were traced. The software calculated the area of each tracing, which then was converted to a droplet radius a. This procedure yielded log–log plots of the mean droplet radius $\langle a \rangle$ versus time t for each quench condition, with the slope being equal to the growth exponent ξ. A typical coarsening experiment lasted 10 min, during which about 10 measurements were taken. For late coarsening times, often there were not 20 droplets discernible on the screen, so in these cases as many droplets as could be seen clearly (which sometimes was as few as 8) were selected for measurement.

The reproducibility of the tracing technique was tested by selecting a single droplet, tracing it, calculating a, erasing the trace, and repeating the measurement 20 times. This test yielded an average a of 9.34 μm with a standard deviation of 0.17 μm, or a relative measurement error of about 2%.

McGuire et al. (1995) started with iPP168-DPE solutions of 10, 15, and 20 wt% iPP168 and quenched to 388, 393, and 398 K. The resulting ϕ values are listed in Table 1. Because iPP138 and iPP120 samples are less viscous than iPP168, they were more prone to "oozing" from between the glass cover slips when heated to 433 K. Thus, it was not possible to use exactly the same experimental conditions for all three iPP–DPE systems. Experimental conditions for the iPP138 and

Table 1
Values of ϕ at quench conditions performed with solutions of iPP–DPE

	10 wt%	12.5 wt%	15 wt%			20 wt%		
	iPP168	iPP138	iPP168	iPP138	iPP120	iPP168	iPP138	iPP120
398 K	0.42	×	×	×	×	×	×	×
393 K	0.54	×	0.32	0.32	0.32	0.23	0.23	0.23
388 K	0.61	×	0.42	0.42	0.42	0.10	0.10	0.10
386 K	×	0.54	×	×	×	×	×	×
380 K	×	0.61	×	×	×	×	×	×
379 K	×	×	×	×	0.54	×	×	×

× = condition not studied.

iPP120 studies were selected to maximize the range of ϕ studied and to match as closely as possible the ϕ values reported by McGuire et al. The conditions and ϕ values used for iPP138 and iPP120 are reported in Table 1, and shown in Fig. 1.

2.2. Determination of physical parameters of iPP–DPE system

Analysis of the coarsening data requires determination of the physical parameters of demixed solutions of iPP–DPE: specifically, the viscosity η of the phase-separated suspension and the interfacial tension γ between the droplet and matrix phases.

2.2.1. Determination of solution viscosities

Suspension viscosities were determined using a Paar Physica Modular Compact Rheometer (MCR300) consisting of a 29 mm-ID cup and 27 mm-OD bob that is concentric with the cup. The MCR300 also includes a solvent trap that consists of a fluid-containing ring that fits snugly around the top of the cup and a sliding plastic cover that clips to the bob shaft. When a measurement is performed on a volatile solution, the ring is filled with the volatile component and the

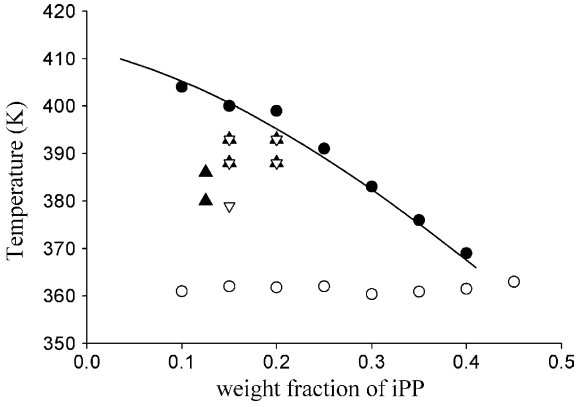

Fig. 1. iPP–DPE phase diagram: (—) theoretical binodal curve, (●) 10 K/min cloud point curve, (○) 10 K/min crystallization curve, (▲) iPP138–DPE quench conditions, (▽) iPP120–DPE quench conditions.

cover is slid down the bob shaft so that the edge of the cover dips into the fluid at all times during the experiment. This creates an atmosphere of the volatile material above the sample, thereby limiting evaporation.

The MCR300 was calibrated with a silicone viscosity standard (RT500, viscosity of 0.484 Pa s at 296 K, obtained from Cannon Instruments). Dynamic testing at $\omega = 10\ s^{-1}$ yielded a complex viscosity of 0.494 Pa s, for a relative measurement error of about 2%.

iPP–DPE samples were prepared by weighting the appropriate amounts of iPP and DPE (totaling approximately 20 g) in a 125 ml Erlenmeyer flask. The flask was purged with nitrogen for at least 20 min and sealed with an aluminum foil-covered cork stopper, and the seal was wrapped tightly with Teflon tape. The contents were slowly heated to 473 K with stirring. After 2 h at 473 K, the flask was immersed in liquid nitrogen and shattered to yield a solid white polymer–diluent sample.

To carry out a measurement, the solvent trap ring was filled with DPE and the MCR300 was heated to 423 K. Finely sliced iPP–DPE sample was added to the heated cup. As the pieces melted, the bob was laid on top of them. After about 2 min, the iPP–DPE pieces had melted sufficiently to allow the bob to sink low enough to make the solvent trap cover dip into the DPE contained in the ring. At that point, the bob was connected to the instrument and the instrument software was used to lower the bob to the measurement position. The sample was sheared at 100 s^{-1} for 4 min to enhance mixing. Then the sample was allowed to sit for 10 min. Finally, the sample was sheared at 200 s^{-1} for 2 min to ensure a consistent initial condition for each experiment. Immediately afterward, the temperature program commenced.

The samples were cooled from 423 to 373 K while being subjected to a harmonic strain. A slow cooling rate (1 K/min) was necessary to avoid overshoot of target temperatures. It was found that a strain amplitude Γ_0 of 1.05 and an angular frequency ω of 20 s^{-1} gave reproducible results for solutions with a weight fraction of iPP of 15% or less; for 20 wt% iPP $\omega = 10\ s^{-1}$ was sufficient. The strain had to be large enough to minimize uncertainty in the measurements. The MCR300 has a standard torque deviation of 0.2 μN m. In order to keep the relative error in the measurements to less than 1%, the torque had to be at least 20 μN m throughout the experiment, and a higher Γ_0 produced a higher torque.

Additionally, the maximum rated torque of the instrument is 150 mN m, and as shown below, crystallization of the polymer at low temperatures increased the torque dramatically. Too high a Γ_0 caused the torque to approach 150 mN m at these temperatures. Too high a ω resulted in stress responses that oscillated wildly because the solution could not react to the strain before the orientation of the strain was reversed.

Studies were performed for 12.5, 15 and 20 wt% iPP138–DPE and iPP120–DPE. After the experiments, it was evident that the duration of the test was short enough to avoid oxidation of the polymer because the sample that came out upon cleaning was still white.

2.2.2. Viscosity results

Since each of the solutions exhibits behavior that is essentially viscous (Martula et al., 2000) and since the Reynolds numbers in demixed iPP–DPE solutions are extremely small ($Re = O(10^{-9})$), it is not necessary to consider non-Newtonian effects here.

Fig. 2 shows viscosity results for iPP138 and iPP120 solutions at three concentrations. In general, the viscosity increases with increasing polymer molecular weight, though this is not true

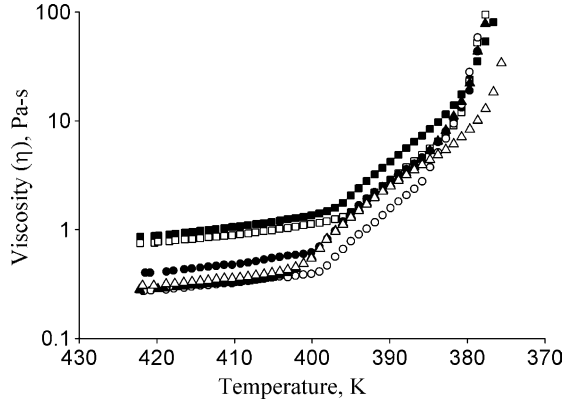

Fig. 2. Viscosity of iPP–DPE systems. 20 wt%: (■) iPP138, (□) iPP120; 15 wt%: (●) iPP138, (○) iPP120; 12.5 wt%: (▲) iPP138, (△) iPP120.

for the 12.5 wt% solutions. However, once phase separation has occurred, all the solutions and matrix phases have viscosity increasing with increasing polymer molecular weight. As any given sample is cooled from 423 K, the polymer solution is above the binodal and homogeneous, so η increases linearly with decreasing temperature. At some temperature (for example, 400 K for the 15 wt% iPP138 solution), η increases dramatically. This change in slope is taken to be indicative of phase separation (Miloh and Beneviste, 1989). Of course, each line of data points has a different break point corresponding to a different phase separation temperature. These phase separation temperatures, plotted in Fig. 3, show excellent agreement with the cloud point measurements and predicted line presented by McGuire et al., and there is no significant molecular weight dependence for the range of molecular weights studied.

The viscosity data shown in Fig. 2 show a second change in slope at a lower temperature. This change in slope is taken to indicate the crystallization of the polymer in the polymer-rich phase.

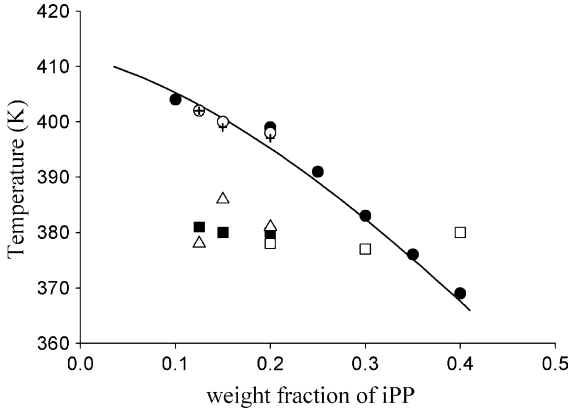

Fig. 3. iPP–DPE phase diagram: (—) theoretical binodal curve, (●) 10 K/min cloud point curve, (○) iPP138 binodal from rheology, (+) iPP120 binodal from rheology, (□) iPP168 crystallization curve from DSC at 2 K/min, (■) iPP138 crystallization curve from rheology, (△) iPP120 crystallization curve from rheology.

The break point temperatures are plotted in Fig. 3 and compared to crystallization data obtained via differential scanning calorimetry (Matsuyama et al., 1998). As expected, the crystallization data obtained via rheological experiments at 1 K/min is slightly above the DSC data, which was obtained at 2 K/min. The rheological data do not indicate any molecular weight dependence of the dynamic crystallization temperature for the range of molecular weights studied here.

To obtain solution viscosities at the conditions of the coarsening experiments, the data in Fig. 2 were extracted at the appropriate polymer concentrations and temperatures. Although the coarsening experiments involved quenching and holding at a specific temperature, it is assumed that the 1 K/min cooling rate used in the dynamic rheological tests was slow enough to approximate the equilibrium values. Some data needed to be extracted at temperatures lower than the polymer crystallization temperature; in these cases the viscosity data were extrapolated to the desired temperature. The extracted values of η are given in Table 2 for iPP138–DPE and iPP120–DPE; any extrapolated values are noted.

2.2.3. Determination of interfacial tensions

In a demixed polymer–diluent system, γ is often very low (less than 1 dyne/cm). This presents a challenge to measuring γ. Experimental methods for determining γ include the sessile drop technique (Nose and Van Tan, 1976; Xia et al., 1992; Haas, 1998), the capillary rise technique (Xia et al., 1992), and spinning drop tensiometry (Heinrich and Wolf, 1992; Laxminarayan, 1994). Laxminarayan (1994) used a spinning drop apparatus, but was unable to measure γ directly for iPP168–DPE due to the high viscosity of the sample. To overcome this difficulty, Laxminarayan measured the surface tensions of the polymer-rich and diluent-rich phases by injecting an air bubble into each phase. To estimate γ indirectly for iPP–DPE, he used Fowkes' relationship (Fowkes, 1964). Laxminarayan obtained interfacial tensions that were O (0.1 dyne/cm), which is comparable to results obtained for polymer solutions (Xia et al., 1992; Haas, 1998; Nose and Van Tan, 1976). However, the Fawkes' relationship is accurate to the nearest 1 dyne/cm at best. As a result, the accuracy of Laxminarayan's method is uncertain. Lacking a reliable experimental technique to use with iPP–DPE, γ was estimated in the current study via experimental observations of the shape relaxations of coalescing droplets.

Hasegawa et al. (in preparation) predicted that the time for a composite droplet to relax to a sphere $t_r \approx K\eta a/\gamma$ where K is a constant and a is the average radius of the two droplets that participate the coalescence event. In CIC simulations performed using this time scaling, K was set

Table 2
Viscosities (in Pa s) of demixed solutions of iPP138–DPE and iPP120–DPE

	12.5 wt%		15 wt%		20 wt%	
	iPP138	iPP120	iPP138	iPP120	iPP138	iPP120
393 K	×	×	1.93 ± 0.04	1.02 ± 0.02	2.80 ± 0.06	1.92 ± 0.04
388 K	×	×	3.60 ± 0.07	2.08 ± 0.04	5.64 ± 0.11	3.70 ± 0.7
386 K	4.50 ± 0.09	×	×	×	×	×
380 K	10.2 ± 0.20*	×	×	×	×	×
379 K	×	×	×	7.00 ± 0.14*	×	×

* = extrapolated data point; × = condition not studied.

to 10, and this choice yielded predictions of the growth exponent ξ in good agreement with the results of McGuire et al. for $\phi \geqslant 0.23$.

During the coarsening experiments, some coalescence events can be seen clearly from start to finish. By observing and timing the shape relaxations of composite droplets, one can estimate t_r, from which γ can be estimated as a function of the quench conditions for both iPP138–DPE and iPP120–DPE. It is acknowledged that without more information about the significance of K, an exact determination of γ cannot be made. However, it is possible to present the results of this method of estimating the interfacial tension in the form of the scaling analysis.

Video recordings of coarsening experiments at the appropriate quench conditions were analyzed to determine γ. At each condition, at least three different pairs of coalescing droplets were studied. When a coalescence event was imminent, the image was frozen and the circumferences of the two participating droplets traced to yield an average radius a. Whenever possible, droplets of approximately equal size were chosen because coalescing droplets of unequal size have a more complex shape relaxation process than equal-sized droplets (Hasegawa et al., in preparation). The tape was restarted and the relaxation time t_r (from first contact until the composite droplet became spherical) was measured with a stopwatch. This procedure was repeated five times for each pair of coalescing droplets studied.

2.2.4. Interfacial tension results

Table 3 shows the temperatures at which relaxation times were observed for each iPP–DPE solution and the corresponding average estimations of γ in units of dyne/cm. Calculating the standard error in the prediction of γ for each quench temperature required including the error in t_r for each composite droplet, the variation in γ resulting from all of the composite droplets studied, and the 2% relative error associated with manually tracing droplet circumferences.

The data from Table 3 is plotted in Fig. 4 and, using the iPP–DPE critical temperature (T_c) of iPP–DPE (Laxminarayan, 1994), in Fig. 5. The slope of the best-fit line through each set of data in Fig. 5 is μ and the intercept is $(1-\kappa)\log(M_w)$. For iPP138–DPE, these lines yield $\mu = 1.13$ and $\kappa = 0.86$; for iPP120–DPE, $\mu = 1.79$ and $\kappa = 0.69$. The interfacial tensions found in this work are compared to those found in other studies with iPP–DPE (Laxminarayan, 1994; Kim et al., 2000) in Fig. 4. Kim et al. used the pendant drop technique to measure surface tensions of the polymer-rich and diluent-rich phases (molecular weight not specified) and Fowkes' relationship to calculate γ. Laxminarayan used the spinning drop technique (M_w of 168,000 g/mole) and the Fawkes' relationship as discussed above. As mentioned above, the Fawkes' relationship is not considered to

Table 3
Estimations of γ for demixed iPP138–DPE and iPP120–DPE solutions

Temperature (K)	iPP138–DPE	iPP120–DPE
393	0.088 ± 0.009	0.054 ± 0.005
388	0.181 ± 0.015	0.133 ± 0.010
386	0.142 ± 0.014	×
380	0.223 ± 0.017	×
379	×	0.236 ± 0.024

× = condition not studied.

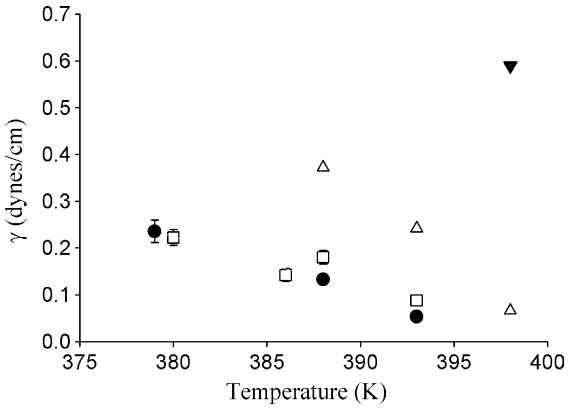

Fig. 4. Estimated interfacial tensions: (□) iPP138–DPE; (●) iPP120–DPE; (△) Laxminarayan (1994); (▼) Kim et al. (2000).

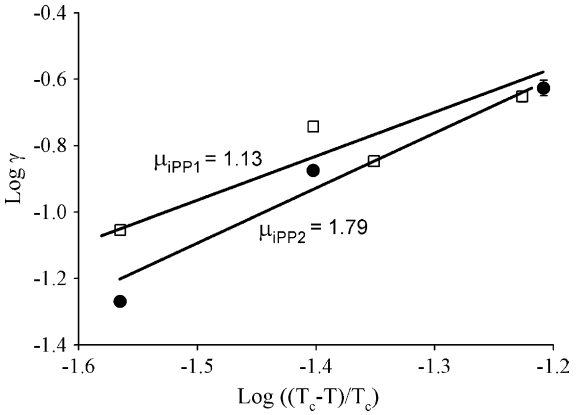

Fig. 5. Scaling plot of interfacial tension for all data obtained: (□) iPP138–DPE; (●) iPP–120–DPE.

be trustworthy for these magnitudes of γ. Given that each set of data was estimated using experimental data generated via different techniques, the differences are not surprising. Regardless of the technique, the results are all of the same order of magnitude. Finally, the results from the present study indicate that the interfacial tension is practically independent of iPP molecular weight for the range of molecular weights studied here.

3. Results and discussion

3.1. Coarsening results

Fig. 6(a)–(f) are log–log representations of the results of the coarsening studies performed by McGuire et al. (1995) and in this work. Data is grouped according to the volume fraction of the

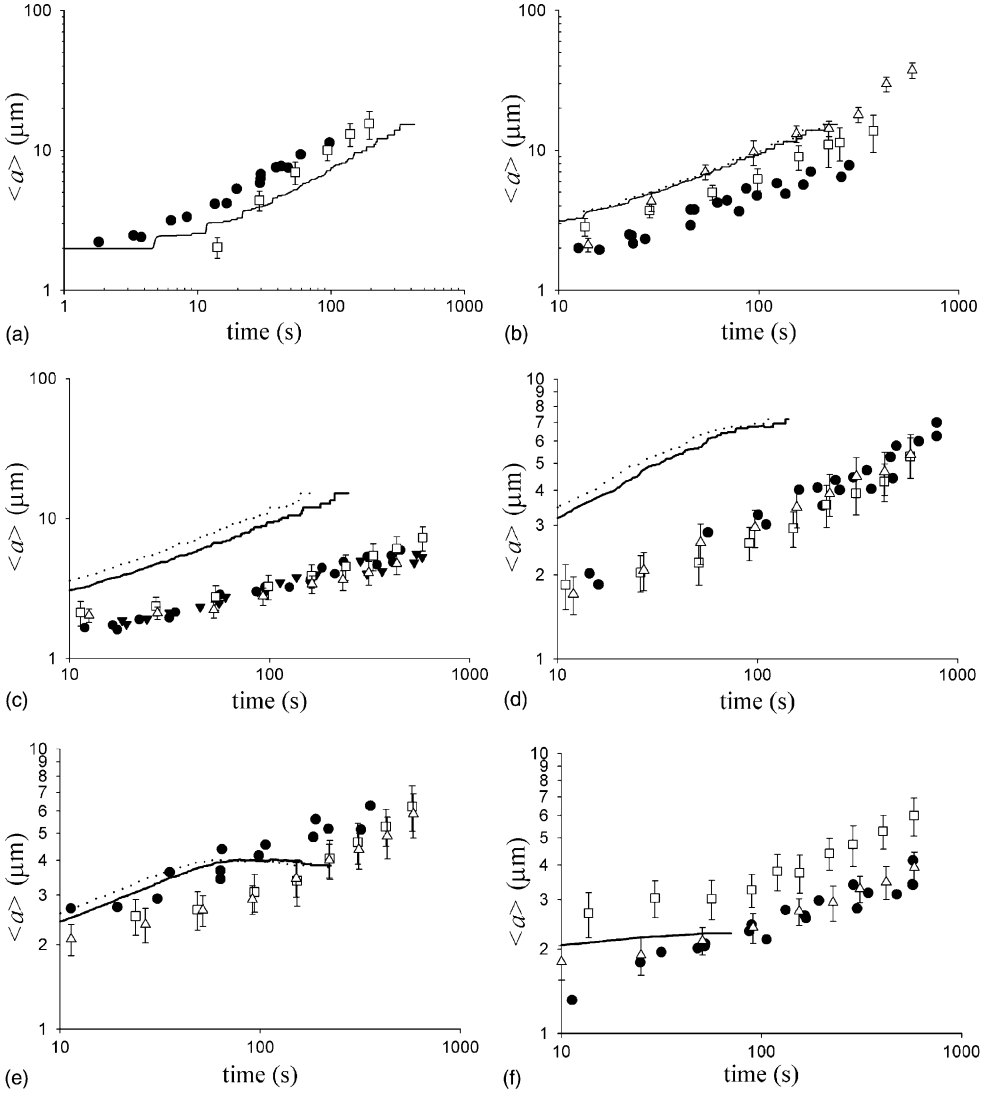

Fig. 6. (a) iPP–DPE coarsening results for $\phi = 0.61$: (●) McGuire et al. (1995) ($\xi = 0.44$, $\sigma_\xi = 0.04$); (□) iPP138–DPE ($\xi = 0.67$, $\sigma_\xi = 0.06$); (—) CIC simulation with $t_r \sim a^2$, $C = 2$, $N_0 = 1372$. (b) iPP–DPE coarsening results for $\phi = 0.54$: (●) McGuire et al. (1995) ($\xi = 0.46$, $\sigma_\xi = 0.06$); (□) iPP138–DPE ($\xi = 0.49$, $\sigma_\xi = 0.06$); (△) iPP120–DPE ($\xi = 0.71$, $\sigma_\xi = 0.09$); (—) iPP138–DPE simulation; (···) iPP120–DPE; both simulations with $t_r \sim a^2$, $C = 2$, $N_0 = 1372$. (c) iPP–DPE coarsening results for $\phi = 0.42$: (▼) McGuire et al. (1995) ($\xi = 0.32$, $\sigma_\xi = 0.03$); (●) McGuire et al. (1995) ($\xi = 0.35$, $\sigma_\xi = 0.03$); (□) iPP138–DPE ($\xi = 0.41$, $\sigma_\xi = 0.06$); (△) iPP120–DPE ($\xi = 0.35$, $\sigma_\xi = 0.04$); (—) iPP138–DPE simulation; (···) iPP120–DPE; both simulations with $t_r \sim a^2$, $C = 2$, $N_0 = 1372$. (d) iPP–DPE coarsening results for $\phi = 0.32$: (●) McGuire et al. (1995) ($\xi = 0.25$, $\sigma_\xi = 0.03$); (□) iPP138–DPE ($\xi = 0.35$, $\sigma_\xi = 0.06$); (△) iPP120–DPE ($\xi = 0.30$, $\sigma_\xi = 0.03$); (—) iPP138–DPE simulation; (···) iPP120–DPE; both simulations with $t_r \sim a^2$, $C = 2$, $N_0 = 1372$. (e) iPP–DPE coarsening results for $\phi = 0.23$: (●) McGuire et al. (1995) ($\xi = 0.22$, $\sigma_\xi = 0.03$); (□) iPP138–DPE ($\xi = 0.34$, $\sigma_\xi = 0.07$); (△) iPP120–DPE ($\xi = 0.36$, $\sigma_\xi = 0.05$); (—) iPP138–DPE simulation; (···) iPP120–DPE; both simulations with $t_r \sim a^2$, $C = 2$, $N_0 = 1372$. (f) iPP–DPE coarsening results for$\phi = 0.10$: (●) McGuire et al. (1995) ($\xi = 0.21$, $\sigma_\xi = 0.03$); (□) iPP138–DPE ($\xi = 0.30$, $\sigma_\xi = 0.04$); (△) iPP120–DPE ($\xi = 0.24$, $\sigma_\xi = 0.03$); (—) iPP138–DPE simulation; (···) iPP120–DPE; both simulations with $t_r \sim a^2$, $C = 2$, $N_0 = 1372$.

droplet phase ϕ, although the exact quench conditions (i.e., temperature and polymer concentration) are not always identical for a given ϕ, and thus emulsion viscosities are different. For McGuire et al.'s data, each point represents a single measurement; for iPP138–DPE and iPP120–DPE, each data point represents the mean of at least three experiments. The error bars represent the standard deviations of the measurements, which were propagated by the 2% relative measurement error in tracing droplet circumferences mentioned above. The growth exponents estimated from the slopes of the data for each ϕ are listed in the legends, along with the deviations in the slopes at 95% confidence (σ_ξ). Notice that ξ is constant over the course of each experiment and increases with increasing ϕ.

The growth exponents for all experiments are plotted as a function of ϕ in Fig. 7. Within experimental error, the ξ values for all three iPP–DPE data sets are in agreement. The data for iPP120 at $\phi = 0.54$ and iPP120 at $\phi = 0.61$ do not at first appear to be in agreement with the previous sentence. However, the apparent discrepancy can be attributed in both cases to the single anomalous data point at $\langle a \rangle \sim 2$ μm. Since McGuire et al. collected more data in the 2–4 μm range than was collected in the present work, one can assume that our data below 4 μm is statistically less reliable than that of McGuire et al.

To convert the results of the CIC simulations to dimensional quantities to compare with the experiments, the initial droplet radius a_0 must be estimated. For each experimental condition, a_0 is obtained by extrapolating to time zero assuming the average droplet radius behaves according to $a_0(1 + kt)^\xi$. The precise value of a_0 has little effect on the growth exponent. It is really only necessary to convert the dimensionless average radius of the droplets from the simulations to the dimensional values for comparison to the experiments.

3.2. Dimensionalization of CIC simulation results

The data given above provides the means to dimensionalize the results of the CIC simulations presented elsewhere (Martula et al., 2000). Dimensionalization of simulated predictions of $\langle a \rangle / a_0$ vs $t\gamma/\eta a_0$ gives predictions of $\langle a \rangle$ vs t that can be compared to the results of the coarsening experiments.

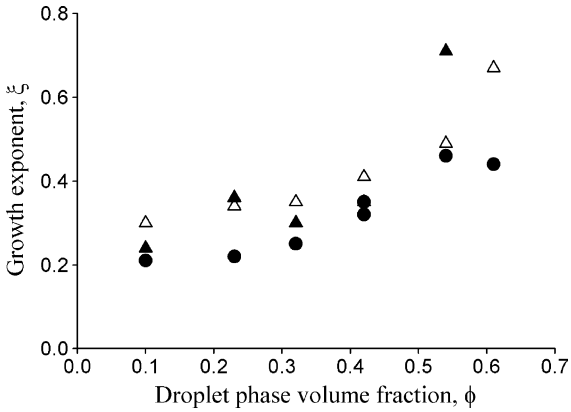

Fig. 7. iPP–DPE growth exponent for all ϕ: (●) McGuire et al. (1995); (△) iPP138–DPE; (▲) iPP120–DPE.

Table 4
Values of the characteristic time $\eta a_0/\gamma$ (ms) for coarsening experiments

	12.5 wt%		15 wt%		20 wt%	
	iPP138	iPP120	iPP138	iPP120	iPP138	iPP120
393 K	×	×	43.2 ± 3.8	34.4 ± 2.4	62.6 ± 5.4	64.8 ± 4.8
388 K	×	×	52.8 ± 3.4	35.8 ± 2.0	82.6 ± 5.2	63.8 ± 3.6
386 K	57.8 ± 4.6	×	×	×	×	×
380 K	94.6 ± 5.2	×	×	×	×	×
379 K	×	×	×	54.2 ± 4.4	×	×

× = condition not studied.

The appropriate values of the interfacial tension γ were calculated using the following scaling relationship (Widom, 1993; Vrij, 1968; Nose and Van Tan, 1976) and estimated values of μ and κ.

$$\gamma \propto M_{\mathrm{w}}^{(1-\kappa)} \left(\frac{T_{\mathrm{c}} - T}{T_{\mathrm{c}}} \right)^{\mu}, \tag{1}$$

where T_{c} is the critical temperature of the system and κ and μ are exponents whose values have been shown experimentally (Shinozaki et al., 1982; Xia et al., 1992; Heinrich and Wolf, 1992; Enders et al., 1995; Haas, 1998) to range from 0.61–0.75 and 1.22–1.5, respectively.

Together with an estimate of 2 μm for a_0, the characteristic time $t_{\mathrm{c}} = \eta a_0/\gamma$ can be calculated for each quench condition; these values are listed in Table 4. The known relative uncertainty in t_{c} is actually less than that of γ because the uncertainty in η that went into the calculation of γ is removed by the inclusion of η in the calculation of t_{c}. The uncertainty in the value of K is incalculable.

From these tables it can be seen that a dimensionless time of 1 corresponds to approximately 60 ms of dimensional coarsening time, depending on η, γ and a_0. Note that t_{c} tends to increase with increasing polymer concentration and decreasing temperature. γ is invariant with the weight fraction of iPP while η increases with polymer concentration, so it makes sense that t_{c} increases with concentration. As the temperature is dropped, both η and γ increase, so the fact that t_{c} tends to increase as T decreases implies that η increases by a greater percentage than γ for a given ΔT.

4. Comparison of simulation results to experimental coarsening results for iPP–DPE

Given estimates of the characteristic time for each quench condition performed in the coarsening experiments, one can dimensionalize the CIC simulation results acquired earlier (Martula et al., 2000). As discussed at length elsewhere (Martula, 2000), the CIC simulation requires specifying the rate of growth or relaxation of the highly curved neck formed by the coalescing droplets. Two models of his process were considered: one where the neck relaxes proportionally to the square of the average radii of the drops ($t_{\mathrm{r}} \sim a^2$) and another where the ring relaxes at rate proportional to the average radius of the drops ($t_{\mathrm{r}} \sim a$). Note also that a dimensionless $O(1)$ constant C for the simulation must be specified as well by matching the predicted and experimentally measured growth exponent at one volume fraction ($\phi = 0.32$). Fig. 8 shows the growth

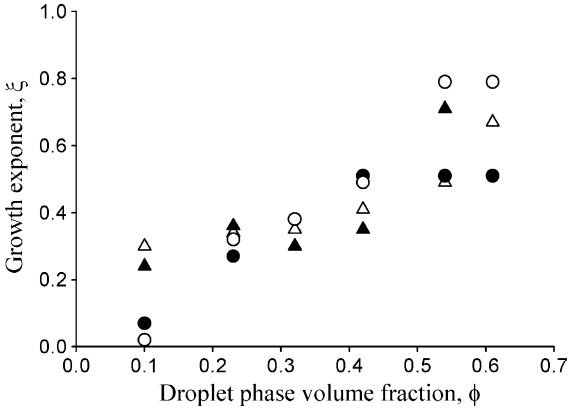

Fig. 8. Comparison of iPP–DPE experimental and estimated growth exponents: (△) iPP138–DPE experiments; (▲) iPP120–DPE experiments, (●) simulation with $t_r \sim a^2$ and $C = 2$; (○) simulation with $t_r \sim a$ and $C = 7$.

exponents predicted by these simulations compared to those found in the coarsening experiments with iPP138–DPE and iPP120–DPE. For the simulation with $t_r \sim a^2$, $C = 2$, agreement with experiment is good for $\phi \geqslant 0.23$, with some underprediction for $\phi \geqslant 0.54$. For the simulation with $t_r \sim a$, $C = 7$, agreement is good for $\phi \geqslant 0.23$, with some overprediction for $\phi \geqslant 0.54$. These comparisons are nearly as satisfactory as those obtained using McGuire et al.'s coarsening data and the original values of C, with the same conclusions: CIC may be at work in emulsions with $\phi \geqslant 0.23$, but it cannot drive coarsening for $\phi < 0.23$.

The volume fraction of about 0.50, where the exponent becomes constant, is similar to the volume fraction value proposed by Nikolayev et al. (1996) for the transition of the growth exponent from 1/3 to unity. However, unlike Nikolayev et al., our maximum growth exponent predicted by theory and measured experimentally is significantly less than one, and the lower values are systematically different from 1/3 at lower droplet concentrations. We have argued previously (Martula et al., 2000) that this transition occurs where the droplets are concentrated enough to allow the hydrodynamics of CIC to propagate in a continuous cascade, which does not quench at lower volume fractions.

Fig. 6(a)–(f) show the experimental data compared to the dimensionalized revised CIC simulation predictions. The results of the CIC simulation for each ϕ were dimensionalized to give $\langle a \rangle$ vs. t predictions for each iPP–DPE system, so for each ϕ two sets of simulation data are plotted. However, for $\phi = 0.10$, the difference in the characteristic time t_c for iPP138–DPE and iPP120–DPE is so slight that the simulation results are indistinguishable for the two systems. At this condition, t_c (iPP138–DPE) = 62.6 and t_c (iPP120–DPE) = 64.8. As a result, a single simulation line in Fig. 6(f) was drawn to represent both sets of dimensionalized simulation results.

Regardless of the agreement between simulation and experiment with respect to ξ, the simulation data does not always line up with the experimental data: growth begins and ends sooner in the simulations, and some simulation results run parallel to instead of on top of the experimental results. However, the fact that γ and a_0 had to be estimated could explain this inconsistency. For instance, if γ were actually an order of magnitude smaller than estimated, the characteristic times calculated in Table 4 would be ten times as great and the simulation data in Fig. 6(a)–(f) would be

shifted to the right by one decade. Clearly, without more information about γ and a_0, it is useless to shift the data arbitrarily in this fashion. Perhaps in the future an experimental technique can be developed to obtain more precise values for each of these parameters.

5. Summary

The technique and results of coarsening experiments with demixed solutions of two molecular weights of iPP combined with DPE were presented. The hypothesis posed in the introduction that changing the M_w of the polymer (and consequently only the solution viscosity η) should not affect the growth exponent ξ for a given ϕ was only weekly shown. The experimental evidence indicates the exponent is not a function of viscosity, supporting the CIC theory.

The growth exponents with iPP138 and iPP120 tended to be equal to or higher than those found by McGuire et al. with their iPP–DPE system (based on 95% confidence), and ξ for iPP138 and iPP120 were close to each other. There may be a difference between McGuire et al.'s experimental techniques and those of this study or perhaps uncharacterized differences between the polymers used.

References

Allcock, H.R., Lampe, F.W., 1990. Contemporary Polymer Chemistry. Prentice-Hall, Inc, Englewood Cliffs, NJ.

Anastasiadis, S.H., Gancarz, I., Koberstein, J.T., 1988. Interfacial tension of immiscible polymer blends: temperature and molecular weight dependence. Macromolecules 21, 2980–2987.

Atkinson, P.M., 1999. Formation of anisotropic flat sheet membranes via evaporative TIPS. Dissertation, The University of Texas at Austin.

Batarseh, M.T., 1999. Formation of anisotropic hollow fiber membranes via TIPS. Dissertation, The University of Texas at Austin.

Beysens, D., 1997. Kinetics and morphology of phase separation in fluids: the role of droplet coalescence. Physica A 239, 329–339.

Binder, K., Stauffer, D., 1976. Statistical theory of nucleation, condensation, and coagulation. Advances in Physics 25, 343–396.

Brown, G., Chakrabarti, A., 1993. Phase separation dynamics in off-critical polymer blends. J. Chemical Physics 98, 2451–2458.

Enders, S., Wolf, B.A., Binder, K., 1995. Interfacial tension of phase-separated polymer solutions and relation to their equation of state. J. Chemical Physics 103, 3809–3819.

Feke, D.L., Schowalter, W.R., 1983. The effect of Brownian diffusion on shear-induced coagulation of colloidal dispersions. J. Fluid Mechanics 133, 17–35.

Fowkes, F.M., 1964. Attractive forces at interfaces. Industrial and Engineering Chemistry 56, 40–52.

Guenon, P., Gastuad, R., Perrot, F., Beysens, D., 1987. Spinodal decomposition in an isodensity critical binary fluid—direct-visualization and light-scattering analysis. Physics Review A 36, 4876.

Haas, C.K., 1998. Coarsening in 2D and 3D phase-separated polymer solutions: implications for microporous membrane morphology. Dissertation, Northwestern.

Hasegawa, T., Martula, D.S., Lloyd, D.R., Bonnecaze, R.T. Coalescence-induced coalescence: calculation of the velocity field. Physics of Fluids, in preparation.

Heinrich, M., Wolf, B.A., 1992. Interfacial tension between solutions of polystyrenes: establishment of a useful master curve. Polymer 33, 1926–1931.

Kim, S.S., Yeom, M.-O., Cho, I.-S., 2000. Thermally-induced phase separation mechanism study for membrane formation. In: Pinnau, I., Freeman, B.D. (Eds.), Membrane Formation and Modification. ACS Press, Washington, pp. 42–64.

Laxminarayan, A., 1994. The kinetics of membrane formation via thermally induced liquid–liquid phase separation. Dissertation, The University of Texas at Austin.

Lifshitz, I.M., Slyozov, V.V., 1961. The kinetics of precipitation from supersaturated solid solutions. J. Physical Chemistry of Solids 19, 33–50.

Lim, G.B.A., 1990. Effects of nucleating agent on thermally induced phase separation membrane formation. Dissertation, The University of Texas at Austin.

Martula, D.S., 2000. Coalescence-induced coalescence. Dissertation, The University of Texas at Austin.

Martula, D.S., Hasegawa, T., Lloyd, D.R., Bonnecaze, R.T., 2000. Coalescence-induced coalescence of inviscid droplets in a viscous fluid. J. Colloid and Interface Science 232, 241–253.

Matsuyama, H., Berghmans, S., Batarseh, M.T., Lloyd, D.R., 1998. Effects of thermal history on anisotropic and asymmetric membranes formed by thermally induced phase separation. J. Membrane Science 142, 27–42.

McGuire, K.S., 1995. Membrane formation via liquid–liquid thermally induced phase separation. Dissertation, The University of Texas at Austin.

McGuire, K.S., Laxminarayan, A., Lloyd, D.R., 1995. Kinetics of droplet growth in liquid–liquid phase separation of polymer–diluent systems: experimental results. Polymer 36, 4951–4960.

McGuire, K.S., Laxminarayan, A., Martula, D.S., Lloyd, D.R., 1996. Kinetics of droplet growth in liquid–liquid phase separation of polymer–diluent systems: model development. J. Colloid and Interface Science 182, 46–58.

Miloh, T., Beneviste, Y., 1989. On the effective viscosity of a nondilute emulsion of two Stokes fluids with small capillary number. Physics of Fluids A 1, 1915–1925.

Nakajima, A., Fujiwara, H., 1968. Phase relationships and thermodynamic interactions in isotactic polypropylene-diluent systems. J. Polymer Science: Part A-2 6, 723–733.

Nikolayev, V.S., Beysens, D., 1997. Coalescence limited by hydrodynamics. Physics of Fluids 9, 3227–3234.

Nikolayev, V.S., Beysens, D., Guenoun, P., 1996. New hydrodynamic mechanism for drop coarsening. Physical Review Letters 76, 3144–3147.

Nose, T., Van Tan, T., 1976. Interfacial tension of demixed polystyrene–methylcyclohexane solution. J. Polymer Science: Polymer Letters Edition 14, 705–712.

Onuki, A., 2002. Phase Transition Dynamics. Cambridge University Press, Cambridge, UK.

Perrot, F., Guenon, P., Baumberger, T., Beysens, D., Garrabos, Y., LeNeidre, B., 1994. Nucleation and growth of tightly packed droplets in fluids. Physics Review Letters 73, 688–691.

Santonicola, G., Mauri, R., Shinnar, R., 2001. Phase separation of initially inhomogeneous liquid mixtures. Industrial and Engineering Chemistry Research 40, 2004–2010.

Shinozaki, K., Abe, M., Nose, T., 1982. Interfacial tension of demixed polymer solutions over a wide range of temperature. Polymer 23, 722–727.

Siggia, E.D., 1979. Late stages of spinodal decomposition in binary mixtures. Physical Review A 20, 595–605.

Song, S.-W., Torkelson, J.M., 1995. Coarsening effects on the formation of microporous membranes produced via thermally induced phase separation of polystyrene–cyclohexanol solutions. J. Membrane Science 98, 209–222.

Tanaka, H., 1994. New coarsening mechanisms for spinodal decomposition having droplet pattern in a binary fluid mixture: collision-induced collision. Physical Review Letters 72, 1702–1705.

Tanaka, H., 1996. Universality of viscoelastic phase separation in dynamically asymmetric fluid mixtures. Physical Review Letters 76, 787–790.

Tanaka, H., Lovinger, A.J., Davis, D.D., 1994. Pattern evolution caused by dynamic coupling between wetting and phase separation in binary liquid mixture containing glass particles. Physical Review Letters 72, 2581–2584.

Troian, S.M., 1993. Coalescence induced domain growth near a wall during spinodal decomposition. Physics Review Letters 71, 1399–1402.

Vrij, A., 1968. Equation for the interfacial tension between demixed polymer solutions. J. Polymer Science: Part A-2 6, 1919–1932.

Wang, H., Davis, R.H., 1995. Simultaneous sedimentation and coalescence of a dilute dispersion of small drops. J. Fluid Mechanics 295, 247–261.

White, W.R., Wiltzius, P., 1995. Real space measurement of structure in phase separating binary fluid mixtures. Physical Review Letters 75, 3012–3015.

Widom, B., 1993. Phase separation in polymer solutions. Physica A 194, 532–541.

Xia, K.-Q., Franck, C., Widom, B., 1992. Interfacial tensions of phase-separated polymer solutions. J. Chemical Physics 97, 1446–1454.

Zhang, X.-G., Davis, R.H., 1991. The rate of collisions due to Brownian or gravitational motion of small drops. J. Fluid Mechanics 230, 479–504.